International Journal of Geo-Information

MDPI

Article

An Object-Oriented Deep Multi-Sphere Support Vector Data Description Method for Impervious Surfaces Extraction Based on Multi-Sourced Data

Yiliang Wan [1,2], Yuwen Fei [1,2], Rui Jin [3,*], Tao Wu [1,2] and Xinguang He [1,2]

1 School of Geographic Sciences, Hunan Normal University, Changsha 410081, China
2 Hunan Key Laboratory of Geospatial Big Data Mining and Application, Changsha 410081, China
3 School of Architecture and Planning, Hunan University, Changsha 410082, China
* Correspondence: ruijin@hnu.edu.cn

Abstract: The effective extraction of impervious surfaces is critical to monitor their expansion and ensure the sustainable development of cities. Open geographic data can provide a large number of training samples for machine learning methods based on remote-sensed images to extract impervious surfaces due to their advantages of low acquisition cost and large coverage. However, training samples generated from open geographic data suffer from severe sample imbalance. Although one-class methods can effectively extract an impervious surface based on imbalanced samples, most of the current one-class methods ignore the fact that an impervious surface comprises varied geographic objects, such as roads and buildings. Therefore, this paper proposes an object-oriented deep multi-sphere support vector data description (OODMSVDD) method, which takes into account the diversity of impervious surfaces and incorporates a variety of open geographic data involving OpenStreetMap (OSM), Points of Interest (POIs), and trajectory GPS points to automatically generate massive samples for model learning, thereby improving the extraction of impervious surfaces with varied types. The feasibility of the proposed method is experimentally verified with an overall accuracy of 87.43%, and its superior impervious surface classification performance is shown via comparative experiments. This provides a new, accurate, and more suitable extraction method for complex impervious surfaces.

Keywords: impervious surface; open geographic data; support vector data description; satellite image; vehicle trajectory

Citation: Wan, Y.; Fei, Y.; Jin, R.; Wu, T.; He, X. An Object-Oriented Deep Multi-Sphere Support Vector Data Description Method for Impervious Surfaces Extraction Based on Multi-Sourced Data. *ISPRS Int. J. Geo-Inf.* **2023**, *12*, 219. https://doi.org/10.3390/ijgi12060219

Academic Editors: Wolfgang Kainz and Wei Huang

Received: 1 March 2023
Revised: 19 May 2023
Accepted: 24 May 2023
Published: 27 May 2023

1. Introduction

Global urbanization is rapidly accelerating, and the urban population is growing at an astonishing rate. As of 2022, 56% of the world's population live in urban areas, and the urban population of the world has surged from 751 million in 1950 to 4.4 billion in 2022 [1]. The urban population boom has led to a significant demand for urban land space, which results in the continued expansion of urban impervious surfaces. Impervious surfaces, such as building roofs, parking lots, and roads, are earth surfaces that prevent water from penetrating into the ground [2,3]. Their physical imperviousness brings a great challenge to the urban ecological environment. The transformation of permeable surfaces to impervious surfaces can negatively impact the urban thermal [4,5] and hydrological environments [6–8]. Therefore, the effective extraction of impervious surfaces is critical to monitor their expansion and ensure the sustainable development of cities.

Remote-sensed images are becoming increasingly important as a data source for impervious surface extraction, owing to their advantages of large-area simultaneous observation, increasingly convenient access, and high spatial resolution. Shao et al. [9] and Cao et al. [10] extracted impervious surfaces by constructing time series of Landsat images. Liu et al. [11] and Misra et al. [12] used Sentinel-2 satellite images to generate the higher-spatial-resolution impervious surface products. Attarchi [13] demonstrated the potential

of Advanced Land Observing Satellite/Phased Array L-band Synthetic Aperture Radar images in impervious surface detection in different urban areas. These studies utilized a single type of optical remote sensing images or radar images and can quickly extract impervious surfaces. However, optical images are susceptible to light and clouds, and radar images are susceptible to speckle noise and geometric deformation, which will affect the accuracy of the model.

The methods integrating multiple remote sensing data sources are proposed to improve impervious surface extraction accuracy. Shao et al. [14] fused Gaofen-1 and Sentinel-1A images to achieve urban impervious surfaces. Guo et al. [15] constructed a multi-feature-based urban impervious surface extraction method based on Sentinel-2 multispectral data and Luojia 1-01 images. Sun et al. [16] extracted impervious surfaces based on the WorldView-2 and airborne LiDAR datasets. These multiple remote sensing data can well compensate for the use of a single image. Impervious surface extraction based on remote sensing is usually combined with machine learning algorithms, such as support vector machines (SVM), random forest, neural networks, and decision tree [17–19]. Despite their effectiveness, most of these machine-learning-based methods require massive training samples, which need to be manually labeled in remote sensing images.

To alleviate the manual workload of labeling impervious surface samples, researchers proposed auto-labeling methods for impervious surface extraction using open geographic data shared by ordinary people or organizations [20]. Mao et al. [21] employed OSM data to eliminate the shading effect of vegetation and improve impervious surface extraction accuracy. Huang et al. [22] used OSM data to assist in the selection of training samples for model training and generated a global artificial impervious surface area dataset at 10 m resolution. Points of Interest (POIs) are also often employed in impervious surface extraction applications [23–25]. In addition, social media data with geographic and human activity characteristics have emerged as another promising source of impervious surface information. Miao et al. [26] generated samples from Twitter and OSM and verified their feasibility for extracting impervious surfaces. Wu et al. [27] integrated Twitter, Weibo, POIs, and OSM data to propose a new impervious surface extraction scheme from synthetic aperture radar images. Vehicle trajectory GPS data have been successfully utilized to generate massive impervious surface samples of road types, which can be used for the automatic extraction of impervious surfaces [28].

Although open geographic data can be important auxiliary data for impervious surface extraction, most of the data are generated on impervious surfaces, resulting in strongly biased samples that only contain impervious surface samples. There exists a serious data imbalance issue where there is only one class of target data in the training sample [29,30]. To address this issue, one-class algorithms, such as one-class support vector machine (OCSVM) and support vector data description (SVDD), have been proposed and applied to impervious surface extraction based on open geographic data and remote-sensed images [26,28,31]. However, these one-class classification methods assume that impervious surface objects comes from a single cluster, which ignores the fact that an impervious surface comprises varied geographic objects, such as roads and buildings. These different types of impervious surfaces present different characteristics involving spectral and texture in remote sensed images.

To overcome the challenge of data multimodality, the concept of multiple hyperspheres is introduced into one-class methods in the field of anomaly detection. Hu et al. [32] proposed a multimodal deep support vector data description (DSVDD) method. This approach constructs multiple hyperspheres to provide a better description for the target class of data for text classification. Zahra et al. [33] proposed a deep multi-sphere support vector data description (DMSVDD) method, which embeds normal data with multimodal distributions into multiple data-packed hyperspheres with minimal volume to generate useful and differentiated features. These methods provide valuable insights for overcoming the limitations of traditional one-class classification methods in handling impervious surface extraction based on open geographic data and remote-sensed images.

Given the difficulty of acquiring massive impervious surface samples with labels and the problem that the traditional one-class classification algorithm is not applicable to multimodal sample data, an object-oriented deep multi-sphere support vector data description (OODMSVDD) method is proposed in this paper. The study aims to integrate multiple open geographic data sources involving OSM, POIs, and vehicle trajectory GPS points to generate impervious surface samples automatically, which will manually reduce the workload of labeling samples. Furthermore, a new one-class classification approach with multiple hyperspheres is explored to improve impervious surface extraction accuracy. The remainder of the paper is organized as follows: The study materials and methods involved in this paper are elaborated in Section 2. Sections 3 and 4 present the experiment setup and experimental results, respectively. The discussion and conclusion are described in Sections 5 and 6.

2. Materials and Methods

2.1. Study Area

For our study, a portion of Shenzhen City was selected as our study area. Shenzhen City is one of the world's most rapidly urbanizing cities and has been ranked as an "Alpha-" city by GaWC 2020 [34]. The study area includes an area of 113.90° E–114.09° E and 22.60° N–22.78° N, mostly belonging to Longhua, Longgang, Nanshan, Baoan, and Guangming districts, as shown in Figure 1.

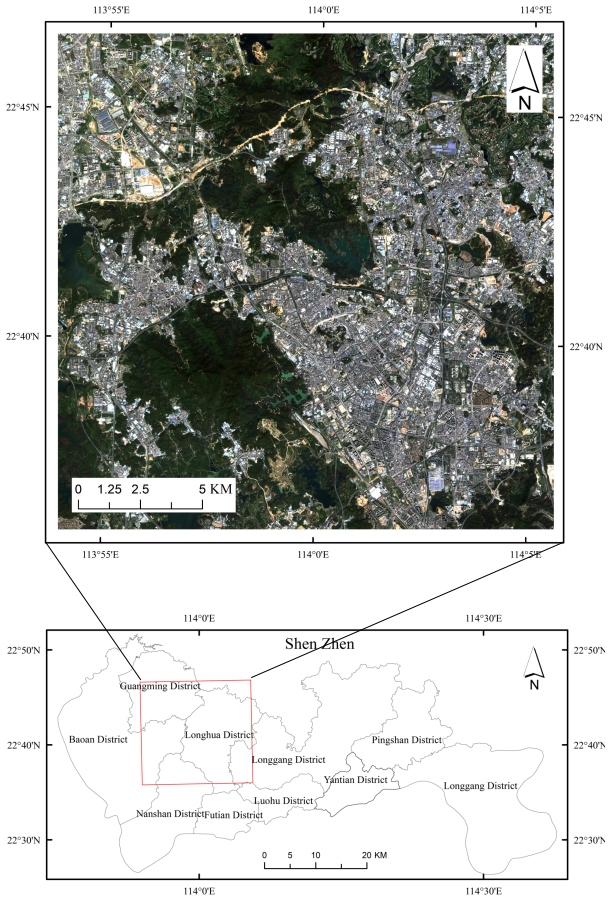

Figure 1. Natural color synthesis of the Gaofen-1 remote sensing image and the location of the study area in Shenzhen City.

2.2. Data Sources

As shown in Figure 1, the experiments in this paper use one panchromatic multispectral image from the Gaofen-1 satellite launched by China. The image was taken on 2 October 2018, and consists of one panchromatic band and four multispectral bands

that were preprocessed and fused into a multispectral image with a 2-meter resolution. The dataset contains 10,000 × 10,000 pixels, covering varied land types, such as water bodies, grasslands, woodlands, artificial buildings, and roads.

Multiple sources of open geographic data, including POIs from Amap (Figure 2a), vehicle trajectory GPS data [35] (Figure 2b), and roads and buildings data from OSM (Figure 2c,d), were collected for this study. These open geographic data are used to automatically generate impervious surface samples. In order to minimize the errors caused by the temporal differences in the data, all the open geographic data were collected in 2018 (Table 1). The POIs were obtained through the Amap API, with a cut-off time of 31 December 2018. The vehicle trajectory GPS data were provided by the Shenzhen Municipal Government Data Open Platform, with a time range from 8 October to 14 October 2018. The road and building data were extracted from OSM data, with a time of 31 December 2018. To verify the accuracy of the proposed method, we manually labeled the impervious and pervious land patches, including roads, buildings, vegetation, and water, etc., based on Google History images in 2018. Furthermore, 10,000 pixel patches consisting of 14 × 14 are selected as the test samples (Figure 2e).

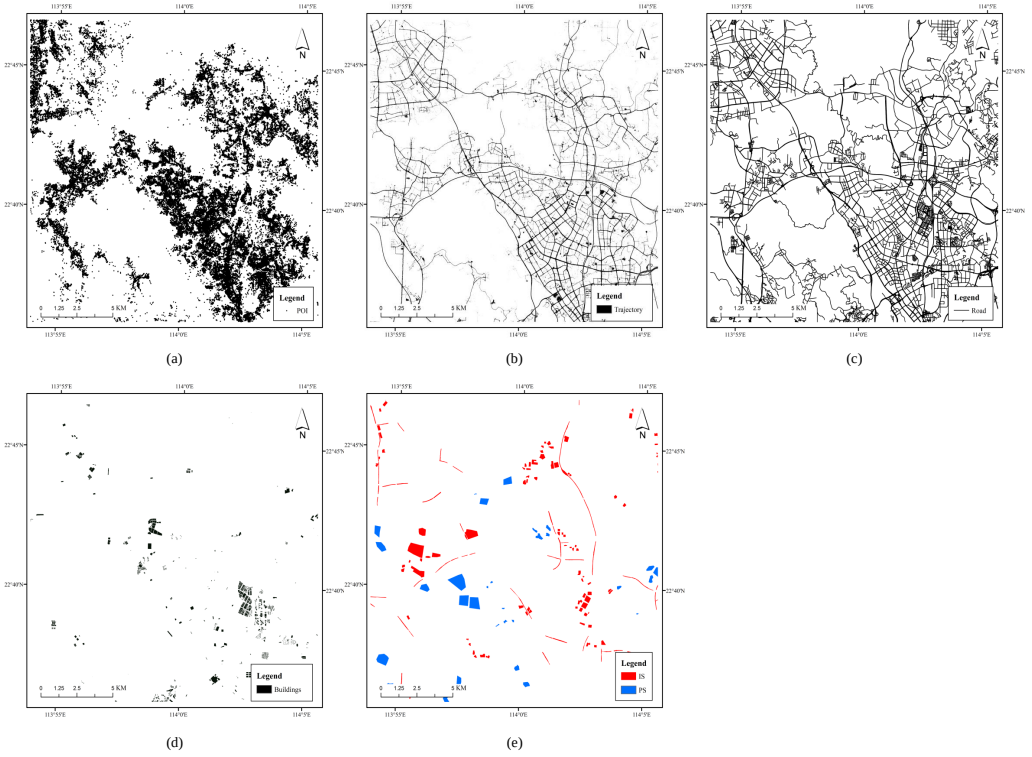

Figure 2. The maps of the datasets in this study. (**a**) POIs from Amap; (**b**) vehicle trajectory GPS points from Shenzhen Municipal Government Data Open Platform; (**c**) roads from OpenStreetMap; (**d**) buildings from OpenStreetMap; (**e**) impervious surface (IS) samples and pervious surface (PS) samples labeled from Google historical images for model validation and testing, which contain various surface coverage types, such as vegetation, water, roads, and buildings.

Table 1. An overview of the collected open geographic datasets.

Data	Time	Source
POIs	31/12/2018	Amap
Vehicle trajectory GPS data	8/10/2018–14/10/2018	Shenzhen Municipal Government Data Open Platform
Roads data	31/12/2018	OpenStreetMap (OSM)
Buildings data	31/12/2018	OpenStreetMap (OSM)

2.3. Methods

2.3.1. Framework

In this paper, an object-oriented automatic extraction method of impervious surface based on DMSVDD is proposed. The technical flow chart of the proposed method is shown in Figure 3. The method consists of five parts: (1) automatic generation of impervious surface samples, which integrates multiple open geographic datasets to generate impervious surface samples; (2) object-oriented training sample processing based on multi-scale segmentation results; (3) construction and training of DSVDD based on single sphere for impervious surface extraction; (4) modeling DMSVDD algorithm for impervious surface extraction that takes into account the diversity of impervious surface types; (5) optimization of impervious surface extraction results based on object blocks.

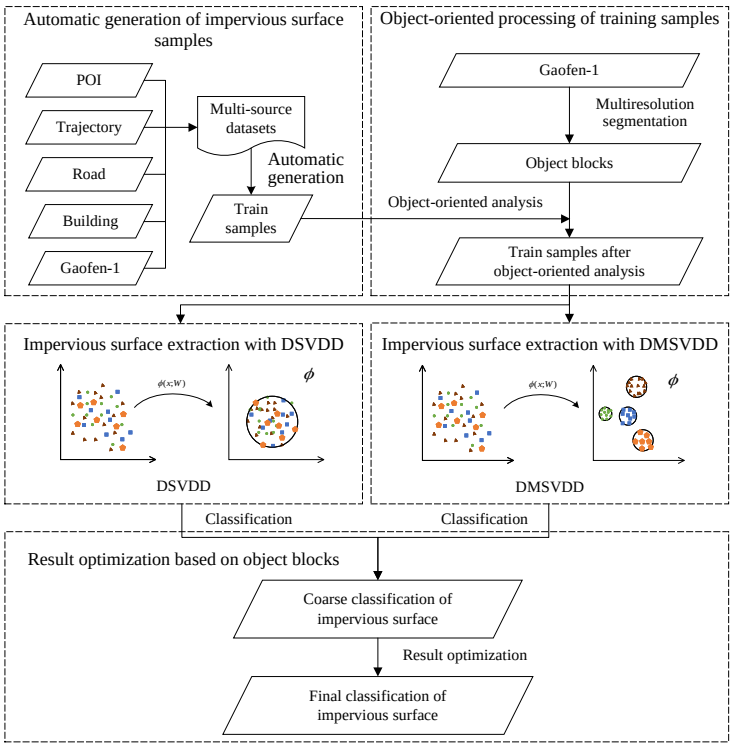

Figure 3. Flowchart of the proposed method.

2.3.2. Automatic Generation of Impervious Surface Samples

Multi-sourced open geographic data are utilized to generate the impervious surface samples with various land cover categories. To ensure consistency with the study area, the datasets are cropped based on the fused GF-1 image and projected to UTM projection with WGS-1984 datum. The data used to generate impervious surface samples include POIs, vehicle trajectory GPS points, and roads and buildings from OpenStreetMap (OSM). To generate impervious surface raster sample data, all the open geographic datasets are classified into two types, including points and polylines or polygons. Two different sample generation methods are developed for these two types of data, respectively (Figure 4). (1) The point datasets including POIs and vehicle trajectory are converted into raster data, the raster image pixel values are computed based on the frequencies of points falling within the pixel, and while there is no point falling in a pixel, the pixel value is set as zero. (2) The roads and buildings data are converted into rasters. We assign a value of "1" for areas with data (i.e., covered by roads or buildings), and areas without data are assigned a value of "0".

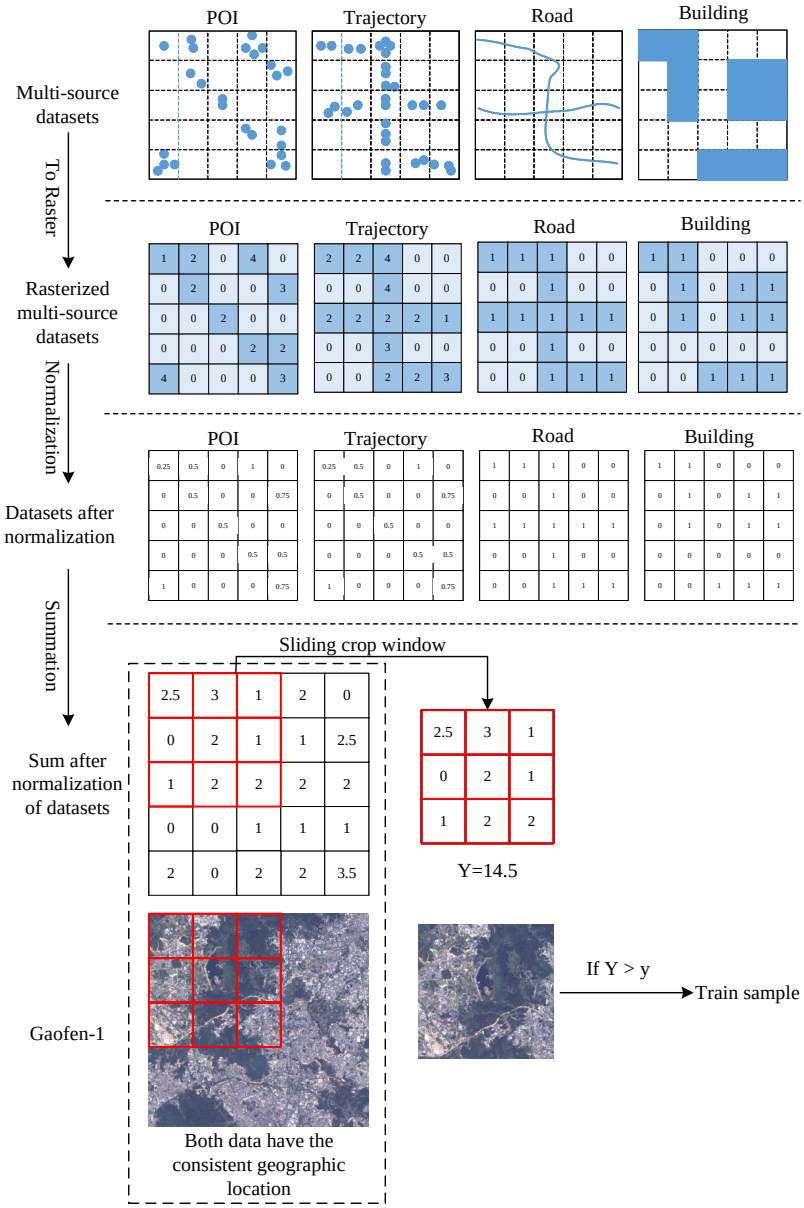

Figure 4. The automatic generation process of training samples from multi-source data.

The more open geographic data generated on impervious surfaces in a certain area, the higher the probability that the area is covered by impervious surfaces. However, due to the users' opportunistic observation efforts, it is inevitable that there exists spatial bias in open geographic data, especially in data shared by ordinary people [36–38]. To address this issue, a threshold method is used to filter the generation of impervious surface samples (Figure 4). Firstly, maximum–minimum normalization is implemented to compress the frequencies of various multi-sourced open geographical data to the interval [0, 1]. Secondly, a sliding window is used to crop the normalized frequency data and remote sensing data. The size of the cropped block is determined based on the network structure of the model. In our paper, the cropped block size is 14 × 14 pixels, and the coverage area is 28 m × 28 m. Thirdly, for each cropped block, its total pixel values are computed and noted as Y, and then a threshold y is set. If Y is not less than the threshold y, then this block has a high probability of being an impervious surface. All pixel blocks that meet the threshold requirements will be used as impervious surface samples to train the impervious surface model.

2.3.3. Object-Oriented Processing of Training Samples

Due to the difference between sample blocks and geographical objects, it is possible that the filtered training samples still contain a small fraction of permeable materials, which are noise samples. In order to eliminate the permeable surface data from the training samples, the object-oriented analysis technique is adopted to process each filtered sample individually. This can make the final training samples as "pure" as possible to reduce the uncertainty brought by noise samples.

Object-oriented analysis techniques can segment remote sensing images into geographical objects as the basic processing unit. In our experiments, we used eCogition software (version 9.0, Trimble Germany GmbH, Munich, Germany, 2014) to segment remote sensing images. The eCogition software is currently one of the most popular tools for image segmentation [39]. For each filtered sample, we performed an object-oriented process, as follows (Figure 5): (1) If the sample block contains only one object block, the sample is used directly for model training; (2) if the sample contains more than one object block, only the image spectral data of the largest object block are retained, while the other regions within the sample are filled with zero values. These samples processed by the object-oriented method are used to train the model.

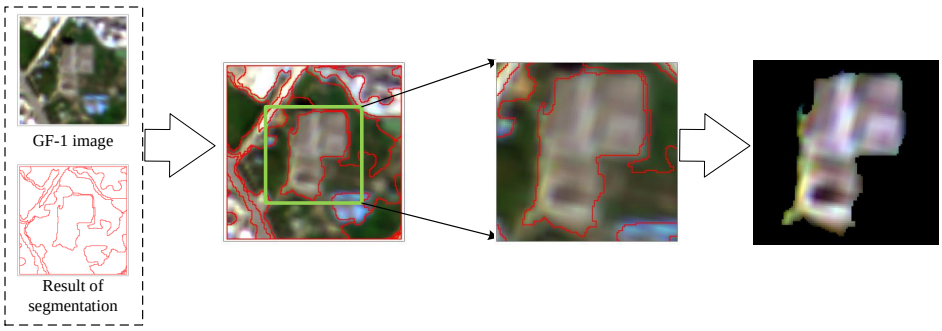

Figure 5. Processing of object-oriented analysis.

2.3.4. Impervious Surface Extraction Based on DSVDD

The DSVDD approach couples SVDD and neural network approaches [40]. One-class classification objective function as in Equation (1) is used by DSVDD to learn the feature representation of an impervious surface, which in turn is used for classification. As shown in Figure 6a, the positive class samples are mapped into an optimal hypersphere during the training process of DSVDD. The hypersphere should be as small as possible and contains as many positive sample points as possible. The sample points falling outside the hypersphere are considered negative classes.

$$\min_{R,\mathcal{W}} R^2 + \frac{1}{vn}\sum_{i=1}^{n}\max\left\{0, \|\phi(x_i;\mathcal{W}) - c\|^2 - R^2\right\} + \frac{\lambda}{2}\sum_{l=1}^{L}\left\|W^l\right\|_F^2 \quad (1)$$

where R denotes the radius of the hypersphere; c is the center of the hypersphere; and the number of samples to be taken is n. $\phi(\cdot;\mathcal{W}) : x \to \mathcal{F}$ represents the neural network, and for sample data $x_i \in \mathcal{X}$ in network ϕ using the $\mathcal{W}$ weight parameter the feature is represented as $\phi(\cdot;\mathcal{W})$, and $\mathcal{W} = \{W^1, \ldots, W^L\}$ is the weight matrix of the network with L hidden layers. Parameter $v \in [0,1]$ is used to control the trade-off between the sphere volume and the boundary. The first part of the formula, $\min_{R,\mathcal{W}} R^2 + \frac{1}{vn}\sum_{i=1}^{n}\max\left\{0, \|\phi(x_i;\mathcal{W}) - c\|^2 - R^2\right\}$, represents a constraint on the hypersphere. The second part $\min_{R,\mathcal{W}} \frac{\lambda}{2}\sum_{l=1}^{L}\left\|W^l\right\|_F^2$ of the equation is a constraint on the network that is used to prevent the network from overfitting.

To determine whether a test sample x_i belongs to the positive or negative class, the DSVDD approach calculates the anomaly score of the sample using Equation (2), where W^* is the weight matrix of the trained neural network.

$$S(x_i) = ||\phi(x_i; W^*) - c||^2 - R^{*2} \tag{2}$$

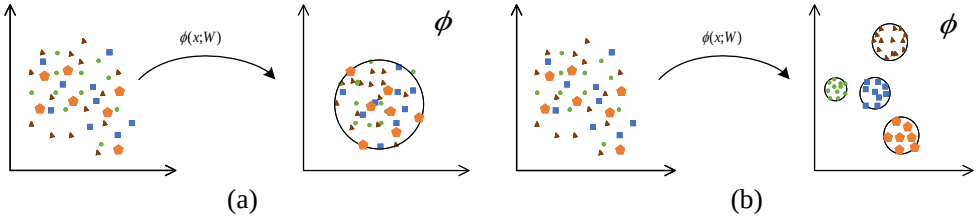

Figure 6. Algorithm diagrams. (**a**) Schematic diagram of DSVDD; (**b**) schematic diagram of DMSVDD.

2.3.5. Impervious Surface Extraction Based on DMSVDD

DMSVDD [33] is an improvement of DSVDD that addresses the tendency of positive class data to exhibit a multimodal distribution (Figure 6b). The idea of DMSVDD lies in embedding the mapping of positive class data with multimodal distribution into multiple data hyperspheres with minimal volume to generate useful data representations. The objective function of DMSVDD is defined as follows.

$$\begin{aligned} \min_{R,\mathcal{W}} \frac{1}{K} \sum_{k=1}^{K} R_k^2 + \frac{1}{vn} \sum_{i=1}^{n} \max\left\{0, \left\|\phi(x_i; \mathcal{W}) - c_j\right\|^2 - R_j^2\right\} \\ + \frac{\lambda}{2} \sum_{l=1}^{L} \left\|W^l\right\|_F^2 \end{aligned} \tag{3}$$

where R, K, and c represent the radius of the hypersphere, the number of hyperspheres, and the center of the hypersphere, respectively. For each sample x_i, assuming that its corresponding hypersphere center is c_j, all hyperspheres are constrained using $\min_{R,\mathcal{W}} \frac{1}{K} \sum_{k=1}^{K} R_k^2 + \frac{1}{vn} \sum_{i=1}^{n} \max\left\{0, \left\|\phi(x_i; \mathcal{W}) - c_j\right\|^2 - R_j^2\right\}$, such that the data are reasonably distributed among multiple hyperspheres, i.e., as many samples as possible fall into multiple spheres and the total volume of all spheres is minimized. The second part $\min_{R,\mathcal{W}} \frac{\lambda}{2} \sum_{l=1}^{L} \left\|W^l\right\|_F^2$ serves the same purpose as the previous section and is used to prevent the network from overfitting.

In the DMSVDD method, the anomaly scores of all the samples also are compared with the trained hypersphere radius to determine the class of the samples. The formula for determining the sample class in DMSVDD is shown in Equation (4), where c_k is the center of the hypersphere to which sample x_i belongs, which is determined according to the nearest neighbor principle. W^* and R^*, respectively, refer to the trained neural network weight matrix and radius.

$$S(x_i) = ||\phi(x_i; W^*) - c_k||^2 - R_k^{*2} \tag{4}$$

2.3.6. Result Optimization Based on Object Blocks

The images to be predicted are fed into the trained model to obtain a classification map, which is considered as the rough impervious surface classification results of OODSVDD or OODMSVDD. A segmented object block as a whole has theoretically consistent classification results. However, due to the network input block size of 14 × 14, which is sometimes smaller than an object block size, and the prediction errors of the neural network model, an object block may be classified as multiple results. To ensure the overall consistency of the object block, object-oriented methods can be applied to optimize the coarse classification results.

To finely correct the classification results using object-oriented methods, we adopt a spatial statistical analysis method. If multiple predicted values occur within a block of objects, the predicted results (impervious surface/permeable surface) covering a larger area of the block are given higher priority. Thus, the predicted labels within an object block are counted and the final labels of that object block are taken according to the predicted label with the largest area within that object block. The resulting classification map represents the final fine classification results of OODSVDD or OODMSVDD after processing as above.

2.3.7. Assessment of Results

In order to verify the feasibility of the proposed method, five metrics commonly used for classification studies are calculated: Overall Accuracy (OA), Precision, Recall, F1-score and Area Under The Curve (AUC). True positive, true negative, false positive, false negative, false positive rate, and true positive rate are denoted as TP, TN, FP, FN, FPR, and TPR, respectively. AUC represents the area under the receiver operating characteristic curve, which is formed by connecting the (FPR, TPR) values of the samples in Cartesian coordinate system. The other metrics are calculated as follows.

$$OA = \frac{TP + TN}{TP + TN + FP + FN} \tag{5}$$

$$Precision = \frac{TP}{TP + FP} \tag{6}$$

$$Recall = \frac{TP}{TP + FN} \tag{7}$$

$$F1 - score = \frac{2TP}{2TP + FP + FN} \tag{8}$$

$$FPR = \frac{FP}{FP + TN} \tag{9}$$

$$TPR = \frac{TP}{TP + FN} \tag{10}$$

3. Experimental Setup and Scenarios

3.1. Experimental Setup

(1) **Filtering threshold for training samples** To determine a reasonable threshold setting range for training sample filtering, the experiments were conducted to count the number of automatically generated training samples under different threshold screening criteria, as shown in Figure 7. It can be found that the number of filtered training samples decreases sharply as the threshold value is set higher. These training samples are obtained by cropping the remote sensing images through sliding windows (Figure 4), and the step of each sliding is set to one half of the sample edge length, so that there is a 50% overlap between two consecutive samples. Therefore, the threshold should not be set too high to ensure that the model training has an adequate number of samples distributed over different geographical locations. If the threshold is set too high, the filtered samples will be overly concentrated in the central, core business district of the city, lacking impervious surface training samples that are slightly out of the central area. Finally, considering the adequacy of the number of samples and the homogeneity of the geographic distribution of samples, five experimental scenarios with thresholds y ($y \in \{10, 20, 30, 40, 50\}$) were set, and 30,000 training samples were randomly selected from the set of samples after threshold screening for model training.

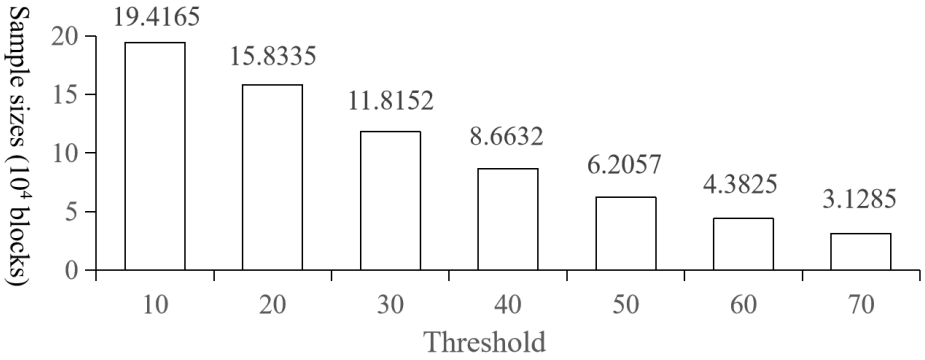

Figure 7. Number of training samples under different threshold values.

(2) **Structure of neural network** According to the basic convolutional network structure, a convolutional neural structure applicable to impervious surface feature extraction is constructed for the DSVDD, DMSVDD, OODSVDD, and OODMSVDD methods in this paper (Figure 8). The input to the network is a three-band block of impervious surface images, with a size of 14 × 14 pixels. The network is made up of a convolutional layer, a pooling layer, and a fully connected layer connection. A convolution kernel of size 5 × 5 is used to extract the local features of the input image, and a filter of size 2 × 2 is used to compute the maximum pooling. Then, these features are flattened to a fully connected layer of 98 nodes. Finally, these features are described by the methods to achieve the classification of samples. The objective functions of the OODSVDD and OODMSVDD networks are shown in Equations (1) and (3), respectively. To achieve the best results, the values of the parameters v and λ are determined by the network parameter tuning.

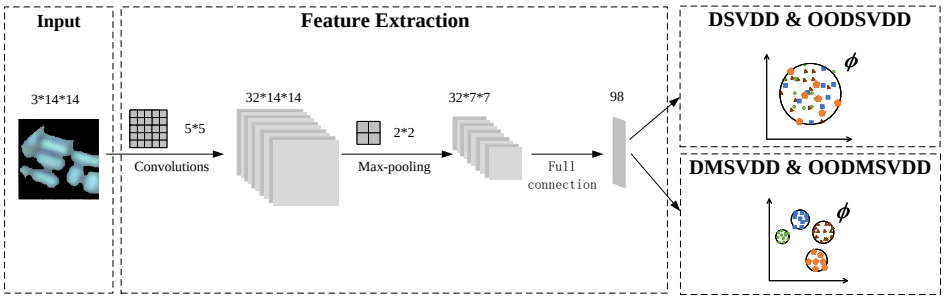

Figure 8. Structure diagram of neural network.

3.2. Experimental Scenarios

In order to test the performance of the proposed method under different conditions, the following three sets of comparison experiments are set up. The performances of all scenarios are evaluated using the average performance of five random seeds and using the same test samples.

(1) **Filtering threshold for training samples** To determine a reasonable threshold setting range for training sample filtering, the experiments are conducted to compute the number of automatically generated training samples under the different thresholds (Figure 7). It can be found that the number of filtered training samples decreases sharply as the threshold value increases. These training samples are obtained by cropping the remote sensing images with a 14 × 14 sliding window (Figure 4), and the step of each sliding is set to one half of the sample edge length. It means that there exists a 50% overlap between two adjacent samples. To train the models, 30,000 samples are randomly selected from the generated impervious surface samples in this study. The sample size will be below 60,000 when the threshold value is greater than 50 at the intervals of 10. Therefore, considering the number and the spatial homogeneity of the samples, five experimental scenarios with thresholds y ($y \in \{10, 20, 30, 40, 50\}$) are set.

(2) **Different methods** A set of control experiments are set up to verify the effectiveness of the object-oriented models involving DSVDD, DMSVDD, and OODMSVDD. For the above three methods, the samples are generated based on the same datasets and from the same region. The only difference is that the training samples of OODMSVDD adopt an object-oriented process (see Section 2.3.3), while the training samples for the DSVDD and DMSVDD methods are generated directly from the multi-sourced geographic data.

(3) **Different data sources** The OODMSVDD model is trained based on samples from five different data sources, and they are combined in this scenario to compare the performances of sample generation from different sources. These datasets include: (a) POIs, (b) buildings from OSM, (c) vehicle trajectory GPS points, (d) roads from OSM, (e) OSM, (f) OSM and vehicle trajectory GPS points, (g) OSM and POIs, (h) POIs and vehicle trajectory GPS points, and (i) all of the above.

4. Results and Analysis

4.1. Experiment 1: Comparison between OODMSVDD and OODSVDD

As shown in Table 2, it can be observed that the OODMSVDD method achieved the best overall results for impervious surface extraction when the threshold value was set to 30 (the map of impervious surface extraction results is shown in Figure 9). The method obtained the highest OA value of 87.43%, while the Precision and Recall values were 84.68% and 91.42%, respectively. Typically, it is challenging to achieve high performance in both the Precision and Recall of a model, so F1-score, the harmonic mean of these two metrics is usually used to evaluate the model's accuracy and recall . The OODMSVDD method achieved the maximum F1-score and AUC values in the experiment, at 87.91% and 92.40%, respectively, when a threshold of 30 was used. This once again demonstrates the excellent performance of the OODMSVDD method for impervious surface extraction when a threshold of 30 is used.

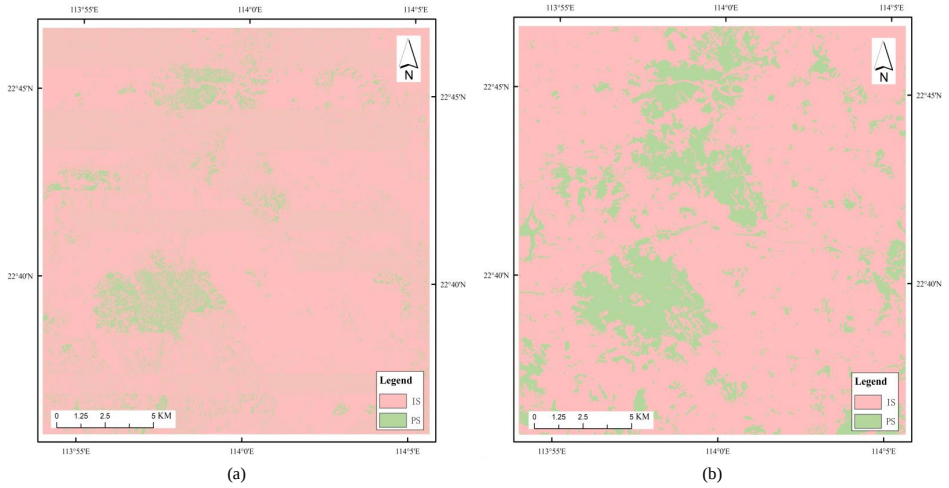

Figure 9. Impervious surface extraction results. (**a**) Coarse impervious surface extraction results for the study area; (**b**) final impervious surface extraction results after object-oriented correction for the study area.

The horizontal comparison of the performance of OODMSVDD and OODSVDD highlights the importance of the number of multi-spheres for the model. A typical demonstration area was selected for the experiment to show the classification results in order to increase the intuitiveness of the model performance at different thresholds, as shown in Figure 10. The experiments show that the Precision and OA of OODMSVDD exceed the corresponding OODSVDD method when the filtering thresholds are 10, 20, 30, and 40, respectively. This indicates that multi-sphere method can improve the Precision and OA of the model in most cases. However, the results differ from the above conclusions when

the threshold value is 50. By analyzing the distribution of training samples at different threshold values, it is found that the samples are mainly concentrated in building types, and the road types cover less when the threshold value is 50. This can affect the accuracy of the model because the roads cover fewer samples. Moreover, most of the building roofs have more consistent surface materials, resulting in a more homogeneous sample data type that is more suitable for single-sphere models. Nevertheless, even in this case, the OA of the multi-sphere model is only 0.62% lower than that of the single-sphere model. Therefore, the OODMSVDD method is more effective for the extraction of impervious surfaces, especially when the impervious surfaces include many different types.

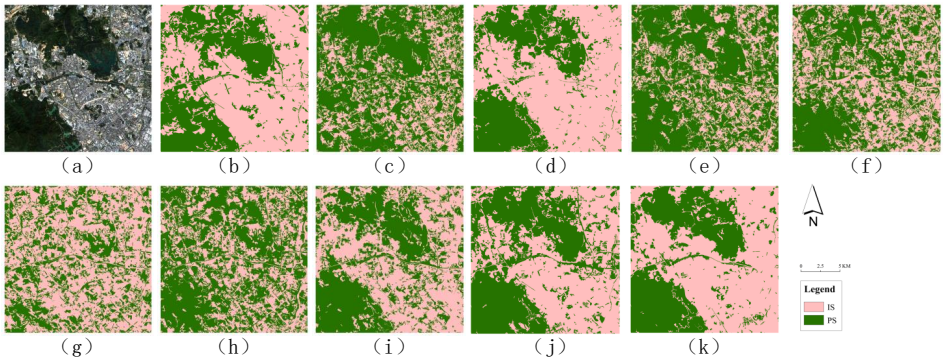

Figure 10. Impervious surface extraction results at different thresholds: (**a**) is the original remote sensed image; (**b**–**f**) are the impervious surface extraction results of OODSVDD thresholds at 10, 20, 30, 40, and 50, respectively; (**g**–**k**) are the impervious surface extraction results of OODMSVDD thresholds at 10, 20, 30, 40, and 50, respectively.

Table 2. Performance in % of impervious surface extraction of OODMSVDD and OODSVDD. The experimental cases with the best comprehensive performance are marked in bold.

Threshold	OODMSVDD					OODSVDD				
	Recall	Precision	OA	F1-Score	AUC	Recall	Precision	OA	F1-Score	AUC
10	93.13	81.63	85.75	86.82	91.19	94.60	79.73	85.19	86.45	90.85
20	90.90	82.75	85.68	86.36	92.15	92.28	81.10	84.93	86.07	91.99
30	**91.42**	**84.68**	**87.43**	**87.91**	**92.40**	**92.66**	**81.81**	**85.90**	**86.84**	**91.53**
40	89.53	81.34	84.21	85.04	90.07	94.00	78.32	83.73	85.29	89.25
50	93.42	79.37	84.16	85.58	90.40	92.70	80.14	84.78	85.93	90.81

4.2. Experiment 2: Comparison between OODMSVDD and DSVDD/DMSVDD

As shown in Table 3, the optimal OA performance of the DSVDD method is 86.95%. Meanwhile, the best OA result for the DMSVDD method is 86.96%. The OA results based on DSVDD and DMSVDD are 0.48% and 0.47% below the optimal OA of 87.43% for the OODMSVDD method, respectively. This indicates that OODMSVDD has better impervious surface extraction performance than DSVDD and DMSVDD, with suitable sample selection. In particular, the best OA results of the multi-sphere methods, including DMSVDD and OODMSVDD, are reached at the sample filtering threshold of 30, while the DSVDD method achieved the highest OA at the threshold of 20. This result proves that the selection of the sample filtering threshold is crucial for the impervious surface extraction, and there exists different optimal thresholds in the multi-sphere SVDD methods and the DSVDD method.

In terms of multi-sphere methods, the results based on the DMSVDD method and the proposed OODMSVDD method are analyzed. The worst classification performance of the DMSVDD method is obtained at a threshold value of 40, and the worst classification OA is 83.68%, which is 0.48% lower than the worst OA of the OODMSVDD method of 84.21%. We observed that the differences between the maximum and minimum results of the five metrics in the OODMSVDD method are smaller than those of the DMSVDD

method. This indicates that the object-oriented analysis method can improve the robustness of the multi-sphere algorithms. Furthermore, the corresponding Recall of the OODMSVDD method is higher than that of the DMSVDD method when the threshold values are 10, 30, and 50. This shows that the object-oriented analysis method can improve the Recall of the model in most cases.

Table 3. Performance in % of impervious surface extraction of OODMSVDD, DMSVDD, and DSVDD. The experimental cases with the best comprehensive performance are marked in bold.

Method	Metrics	Threshold				
		10	20	30	40	50
DSVDD	Recall	89.83	**91.03**	89.68	89.86	93.42
	Precision	81.52	**84.22**	84.36	83.91	82.53
	OA	84.61	**86.95**	86.33	86.00	86.66
	F1-Score	85.39	**87.45**	86.80	86.59	87.57
	AUC	90.95	**92.90**	92.39	91.79	91.92
DMSVDD	Recall	88.67	92.35	**88.11**	91.00	89.10
	Precision	84.22	82.80	**86.56**	79.60	83.91
	OA	85.76	86.54	**86.96**	83.68	85.94
	F1-Score	86.16	87.30	**87.14**	84.83	86.33
	AUC	91.66	92.35	**93.84**	89.58	91.92
OODMSVDD	Recall	93.13	90.90	**91.42**	89.53	93.42
	Precision	81.63	82.75	**84.68**	81.34	79.37
	OA	85.75	85.68	**87.43**	84.21	84.16
	F1-Score	86.82	86.36	**87.91**	85.04	85.58
	AUC	91.19	92.15	**92.40**	90.07	90.40

4.3. Experiment 3: Evaluation of OODMSVDD Based on Different Data Sources

Table 4 presents the classification performance based on different data sources. It reveals that combining multiple sources of data to automatically generate training samples yields the best results for impervious surface extraction. When considering using only one type of data, the POI-data-based impervious surface classification results have the highest Precision, OA, F1-Score, and AUC scores. However, the Recall is the lowest in this case, differing from the highest by 7.55%. On the other hand, the extraction results based on building data rank low in all metrics except Recall. This is because the roofs of buildings are covered with various objects, including impervious surfaces, such as concrete and asphalt, in addition to permeable surface constituents, such as natural moss and artificially planted greenery on some old residential buildings. This leads to the inclusion of permeable surface features in the training samples. This will make the model inaccurately learn the features for impervious surfaces, ultimately resulting in the low accuracy and high recall of the model.

Compared to the road dataset, the model trained based on the vehicle trajectory GPS points shows better performance for all metrics. Meanwhile, the model trained with the road data has poorer overall performance for the impervious surface extraction. The Precision and Recall of the models based on the trajectory GPS data samples are relatively balanced, achieving higher scores for both F1-Score and AUC compared to the road data. This is because the trajectory GPS data cover a wider range of roads than the OSM road data. The trajectory data are collected by vehicle GPS, which can provide more comprehensive, realistic, and timely road data. Therefore, although both training samples can be used to generate road samples, the model based on trajectory GPS data achieves better results in impervious surface extraction than road data from OSM.

Table 4. The performance in % of impervious surfaces is extracted with samples generated using different open geographic data. The experimental cases with the best comprehensive performance are marked in bold.

Data	Recall	Precision	OA	F1-Score	AUC
POI	85.31	87.44	86.52	86.34	93.18
Building	91.20	78.73	83.03	84.38	88.69
Trajectory GPS	90.07	81.40	84.63	85.42	89.76
Road	92.86	77.16	82.49	84.22	87.40
OSM	88.76	83.90	85.39	85.93	91.46
OSM+Trajectory GPS	91.78	79.27	83.62	84.99	89.06
OSM+POI	89.69	85.71	87.23	87.53	93.08
POI+Trajectory GPS	91.70	83.48	86.74	87.38	93.14
All of the above	**91.42**	**84.68**	**87.43**	**87.91**	**92.40**

When two or three data types are used to generate samples to train the model, the impervious surface extraction results are comprehensively better than using a single data source. When POI is overlaid with any kind of data, the model achieves better impervious surface extraction performance. The reason for this may be that POI data cover more types of impervious surface samples than other data and therefore can improve the model results for other data. When the four data types mentioned above are combined to generate samples, the impervious surface extraction achieves the best overall performance with an OA of 87.43%, and the Recall and Precision are well balanced. This demonstrates that each type of the datasets can produce different kinds of information on impervious surfaces and complement each other to improve the results. In addition, samples generated from multiple data sources are more suitable for the multi-sphere algorithm.

5. Discussion

To investigate the performance of the proposed method for impervious surface extraction with different training sample sizes, we vary the sample size between 10,000 and 40,000, with an interval of 10,000. The top-ranked result of each threshold has been bolded. The results in Table 5 demonstrate that the model consistently achieves the best classification performance when the threshold value is set to 30, regardless of the sample size variation. Conversely, when the threshold is set to 10 or 50, the classification performance of the proposed method suffers. This is attributed to the presence of noisy data in the impervious surface samples generated from the multi-sourced open geographic data. A low threshold fails to effectively filter out irrelevant training samples, which in turn reduces the accuracy of impervious surface extraction. On the other hand, a high threshold filters out training samples with high impervious surface probability. This can result in a reduction in the diversity of impervious surface samples and consequently affect the model results. Hence, it is essential to determine an appropriate threshold for filtering the training samples.

The overall performance of the model is stable for a fixed threshold, with similar overall accuracies (OA) observed at sample sizes of 20,000, 30,000, and 40,000. The best classification accuracy is usually achieved with sample sizes of 20,000 or 30,000, while the worst is achieved with a sample size of 10,000. The metrics scores of the model show that the lack of information leads to a low precision due to small sample size. However, when the sample size is large enough and contains enough information, the accuracy of the proposed model does not change significantly with the increase in the number of samples. This feature facilitates the extension of the proposed method for impervious surface extraction in areas with few training samples generated from multiple sources of data.

Table 5. Classification performance in % of OODMSVDD with different training sample sizes and thresholds. The experimental cases with the best comprehensive performance are marked in bold.

Threshold	Metrics	Sample Size ($\times 10^3$ blocks)			
		10	**20**	**30**	**40**
10	Recall	90.44	93.26	**93.13**	91.12
	Precision	68.40	78.91	**81.63**	77.23
	OA	74.10	83.95	**85.75**	81.05
	F1-Score	77.78	85.38	**86.82**	82.85
	AUC	77.32	89.64	**91.19**	87.69
20	Recall	92.05	**94.65**	90.90	90.93
	Precision	72.08	**80.68**	82.75	81.09
	OA	77.94	**85.78**	85.68	84.63
	F1-Score	80.75	**87.01**	86.36	85.60
	AUC	85.16	**91.80**	92.15	91.77
30	Recall	92.72	91.92	**91.42**	91.50
	Precision	71.70	83.12	**84.68**	81.74
	OA	78.00	86.58	**87.43**	85.31
	F1-Score	80.84	87.25	**87.91**	86.23
	AUC	85.93	91.81	**92.40**	91.27
40	Recall	91.81	**91.31**	89.53	91.33
	Precision	68.90	**82.22**	81.34	80.79
	OA	75.00	**85.71**	84.21	84.46
	F1-Score	78.66	**86.49**	85.04	85.57
	AUC	80.68	**91.44**	90.07	90.20
50	Recall	90.71	89.40	**93.42**	89.44
	Precision	67.73	80.78	**79.37**	81.06
	OA	73.71	83.00	**84.16**	84.13
	F1-Score	77.54	84.14	**85.58**	84.93
	AUC	79.65	91.61	**90.40**	89.73

6. Conclusions

In the context of rapid urbanization, it is crucial to develop an effective impervious surface extraction method for monitoring changes in urban ground cover materials. The increase in impervious surfaces poses significant challenges to the health of cities. In this paper, we propose an object-oriented deep multi-sphere support vector data description (OODMSVDD) method that considers multiple types of impervious surfaces. Our approach uses multiple sources of data, such as vehicle trajectories and OSM, to automatically generate single-class impervious surface samples. This greatly reduces the burden of the manual labeling of training samples. We employ object-oriented analysis techniques and extend the number of support vector data description (SVDD) spheres to improve the accuracy and robustness of the impervious surface extraction model. Our improved model is better suited to extract impervious surfaces consisting of diverse geographic objects.

The use of multi-source data to address the challenge of acquiring labeled samples in impervious surface extraction has yielded promising results. They show that it is essential to filter the training samples using a suitable method, such as a threshold method employed in this study. Furthermore, selecting a moderate number of training samples can strike a balance between sample size and better classification results. Even in situations where data sources are insufficient, the proposed method can still achieve relatively good results for impervious surface extraction. However, there is a need for further research on the impact of data uncertainty, such as position drift in trajectory data, POI localization errors, and other issues. Additionally, exploring a precise method to filter the automatically generated training samples and reduce the impact of data uncertainty on the results will be a focus of future researches.

Author Contributions: All authors made significant contributions to this study. Conceptualization, Yiliang Wan and Rui Jin; methodology, Yuwen Fei and Yiliang Wan.; software, Yuwen Fei and Yiliang Wan; validation, Tao Wu, Xinguang He, and Rui Jin; formal analysis, Yuwen Fei and Yiliang Wan; resources, Yiliang Wan and Rui Jin; writing—original draft preparation, Yuwen Fei and Yiliang Wan; writing—review and editing, Rui Jin, Yiliang Wan, and Tao Wu; funding acquisition, Yiliang Wan, Yuwen Fei and Rui Jin. All authors have read and agreed to the published version of the manuscript.

Funding: This work is supported by the National Natural Science Foundation of China (grant number: 42271486 and 42101438); Humanity and Social Science Youth foundation of Ministry of Education of China (grant number: 21YJCZH151 and 20YJC790055); Hunan Province Natural Science Foundation, China (grant number: 2022JJ30391 and 2020JJ5051); Changsha City Outstanding Innovative Youth Training Program, China (grant number: kq2009017); and the Postgraduate Scientific Research Innovation Project of Hunan Province, China (grant number: CX20210477).

Data Availability Statement: The original Gaofen-1 product used in this study were obtained from China Centre for Resource Satellite Data and Application (https://data.cresda.cn) (accessed on 9 July 2021). OSM data and trajectory GPS data were obtained from OpenStreetMap (https://openstreetmap.org) (accessed on 18 October 2022) and Shenzhen Municipal Government Data Open Platform (https://opendata.sz.gov.cn/) (accessed on 2 August 2019), respectively. POI data were provided by AMap.

Conflicts of Interest: The authors declare no conflict of interest.

References

1. World Bank. Urban Development. Available online: https://www.worldbank.org/en/topic/urbandevelopment/overview (accessed on 25 December 2022).
2. Gong, P.; Li, X.; Zhang, W. 40-Year (1978–2017) Human Settlement Changes in China Reflected by Impervious Surfaces from Satellite Remote Sensing. *Sci. Bull.* **2019**, *64*, 756–763. [CrossRef] [PubMed]
3. Arnold, C.L., Jr.; Gibbons, C.J. Impervious Surface Coverage: The Emergence of a Key Environmental Indicator. *J. Am. Plan. Assoc.* **1996**, *62*, 243–258. [CrossRef]
4. Derdouri, A.; Wang, R.; Murayama, Y.; Osaragi, T. Understanding the Links between LULC Changes and SUHI in Cities: Insights from Two-Decadal Studies (2001–2020). *Remote Sens.* **2021**, *13*, 3654. [CrossRef]
5. LI, H. Spatiotemporal Dynamics and Thermal Environment Effects of Urban Impervious Surfaces in Xuzhou. Master's Thesis, China University of Mining and Technology, Beijing, China, 2020.
6. Hou, Y.; Ding, W.; Liu, C.; Li, K.; Cui, H.; Liu, B.; Chen, W. Influences of Impervious Surfaces on Ecological Risks and Controlling Strategies in Rapidly Urbanizing Regions. *Sci. Total Environ.* **2022**, *825*, 153823. [CrossRef]
7. Bonneau, J.; Fletcher, T.D.; Costelloe, J.F.; Burns, M.J. Stormwater infiltration and the 'urban karst'—A review. *J. Hydrol.* **2017**, *552*, 141–150. [CrossRef]
8. Yang, K.; Pan, M.; Yang, R.; Song, Y.; Meng, C. Water environmental impacts of impervious surfaces and control measures in Dianchi Lake Basin, China. *Chin. J. Environ. Eng.* **2016**, *10*, 5407–5412.
9. Shao, Z.; Pan, Y.; Cai, Y.; Shu, Y.; Wang, H. Remote Sensing Monitoring of Impervious Surface in Wuhan City Based on Landsat Imagery. *Geospat. Inf.* **2018**, *16*, 1–5+7.
10. Cao, X.; Gao, X.; Shen, Z.; Li, R. Expansion of Urban Impervious Surfaces in Xining City Based on GEE and Landsat Time Series Data. *IEEE Access* **2020**, *8*, 147097–147111. [CrossRef]
11. Liu, Y.; Wu, Y.; Chen, Z.; Huang, M.; Du, W.; Chen, N.; Xiao, C. A Novel Impervious Surface Extraction Method Based on Automatically Generating Training Samples From Multisource Remote Sensing Products: A Case Study of Wuhan City, China. *IEEE J. Sel. Top. Appl. Earth Obs. Remote Sens.* **2022**, *15*, 6766–6780. [CrossRef]
12. Misra, M.; Kumar, D.; Shekhar, S. Assessing Machine Learning Based Supervised Classifiers For Built-Up Impervious Surface Area Extraction From Sentinel-2 Images. *Urban For. Urban Green.* **2020**, *53*, 126714. [CrossRef]
13. Attarchi, S. Extracting Impervious Surfaces from Full Polarimetric SAR Images in Different Urban Areas. *Int. J. Remote Sens.* **2020**, *41*, 4642–4661. [CrossRef]
14. Shao, Z.; Fu, H.; Fu, P.; Yin, L. Mapping Urban Impervious Surface by Fusing Optical and SAR Data at the Decision Level. *Remote Sens.* **2016**, *8*, 945. [CrossRef]
15. Guo, X.; Zhang, C.; Luo, W.; Yang, J.; Yang, M. Urban Impervious Surface Extraction Based on Multi-Features and Random Forest. *IEEE Access* **2020**, *8*, 226609–226623. [CrossRef]
16. Sun, Z.; Zhao, X.; Wu, M.; Wang, C. Extracting Urban Impervious Surface from WorldView-2 and Airborne LiDAR Data Using 3D Convolutional Neural Networks. *J. Indian Soc. Remote Sens.* **2019**, *47*, 401–412. [CrossRef]
17. Abdi, A.M. Land Cover and Land Use Classification Performance of Machine Learning Algorithms in a Boreal Landscape Using Sentinel-2 Data. *Gisci. Remote. Sens.* **2020**, *57*, 1–20. [CrossRef]

18. Bian, J.; Li, A.; Zuo, J.; Lei, G.; Zhang, Z.; Nan, X. Estimating 2009–2017 Impervious Surface Change in Gwadar, Pakistan Using the HJ-1A/B Constellation, GF-1/2 Data, and the Random Forest Algorithm. *ISPRS Int. J. Geo-Inf.* **2019**, *8*, 443. [CrossRef]
19. Hu, D.; Chen, S.; Qiao, K.; Cao, S. Integrating CART Algorithm and Multi-Source Remote Sensing Data to Estimate Sub-Pixel Impervious Surface Coverage: A Case Study from Beijing Municipality, China. *Chin. Geogr. Sci.* **2017**, *27*, 614–625. [CrossRef]
20. Estima, J.; Painho, M. User Generated Spatial Content-Integrator: Conceptual Model to Integrate Data from Diverse Sources of User Generated Spatial Content. *ISPRS Int. Geo-Inf.* **2016**, *5*, 183. [CrossRef]
21. Mao, T.; Fan, Y.; Zhi, S.; Tang, J. A Morphological Feature-Oriented Algorithm for Extracting Impervious Surface Areas Obscured by Vegetation in Collaboration with OSM Road Networks in Urban Areas. *Remote Sens.* **2022**, *14*, 2493. [CrossRef]
22. Huang, X.; Yang, J.; Wang, W.; Liu, Z. Mapping 10 m Global Impervious Surface Area (GISA-10m) Using Multi-Source Geospatial Data. *Earth Syst. Sci. Data* **2022**, *14*, 3649–3672. [CrossRef]
23. Chen, Y.; Ge, Y.; An, R.; Chen, Y. Super-Resolution Mapping of Impervious Surfaces from Remotely Sensed Imagery with Points-of-Interest. *Remote Sens.* **2018**, *10*, 242. [CrossRef]
24. Yu, Y.; Li, J.; Zhu, C.; Plaza, A. Urban Impervious Surface Estimation from Remote Sensing and Social Data. *Photogramm. Eng. Remote Sens.* **2018**, *84*, 771–780. [CrossRef]
25. Fan, W.; Wu, C.; Wang, J. Improving Impervious Surface Estimation by Using Remote Sensed Imagery Combined With Open Street Map Points-of-Interest (POI) Data. *IEEE J. Sel. Top. Appl. Earth Obs. Remote Sens.* **2019**, *12*, 4265–4274. [CrossRef]
26. Miao, Z.; Xiao, Y.; Shi, W.; He, Y.; Gamba, P.; Li, Z.; Samat, A.; Wu, L.; Li, J.; Wu, H. Integration of Satellite Images and Open Data for Impervious Surface Classification. *IEEE J. Sel. Top. Appl. Earth Obs. Remote Sens.* **2019**, *12*, 1120–1133. [CrossRef]
27. Wu, W.; Miao, Z.; Xiao, Y.; Li, Z.; Zang, A.; Samat, A.; Du, N.; Xu, Z.; Gamba, P. New Scheme for Impervious Surface Area Mapping From SAR Images With Auxiliary User-Generated Content. *IEEE J. Sel. Top. Appl. Earth Observ. Remote Sens.* **2020**, *13*, 5954–5970. [CrossRef]
28. Wan, Y.; Fei, Y.; Wu, T.; Jin, R.; Xiao, T. A Novel Impervious Surface Extraction Method Integrating POI, Vehicle Trajectories, and Satellite Imagery. *IEEE J. Sel. Top. Appl. Earth Obs. Remote Sens.* **2021**, *14*, 8804–8814. [CrossRef]
29. Feng, A.; Chen, S. Study on One-Class Classifiers Based On Kernel Method. *J. Nanjing Norm. Univ. Eng. Technol. Ed.* **2008**, *8*, 1–6.
30. Feng, A.; Chen, B. Improved LP Algorithms of One-Class Classifier Based on Local Density Factor. *J. Nanjing Univ. Aeronaut. Astronaut.* **2006**, *38*, 727–731.
31. Xu, Z.; Mountrakis, G.; Quackenbush, L.J. Impervious surface extraction in imbalanced datasets: Integrating partial results and multi-temporal information in an iterative one-class classifier. *Int. J. Remote Sens.* **2017**, *38*, 43–63. [CrossRef]
32. Hu, C.; Feng, Y.; Kamigaito, H.; Takamura, H.; Okumura, M. One-class Text Classification with Multi-modal Deep Support Vector Data Description. *J. Nat. Lang. Process.* **2021**, *28*, 1053–1088. [CrossRef]
33. Ghafoori, Z.; Leckie, C. Deep Multi-sphere Support Vector Data Description. In Proceedings of the 2020 SIAM International Conference on Data Mining, Cincinnati, OH, USA, 7–9 May 2020.
34. Geography Department at Loughborough University. The World According to GaWC 2020. Available online: https://www.lboro.ac.uk/microsites/geography/gawc/world2020t.html (accessed on 15 October 2022).
35. Transportation Bureau of Shenzhen Municipality. Shenzhen Municipal Government Data Open Platform. Available online: https://opendata.sz.gov.cn/ (accessed on 2 August 2019).
36. Wu, H.; Lin, A.; Clarke, K.C.; Shi, W.; Cardenas-Tristan, A.; Tu, Z. A Comprehensive Quality Assessment Framework for Linear Features from Volunteered Geographic Information. *Int. J. Geogr. Inf. Sci.* **2021**, *35*, 1826–1847. [CrossRef]
37. Yamashita, J.; Seto, T.; Nishimura, Y.; Iwasaki, N. VGI Contributors' Awareness of Geographic Information Quality and Its Effect on Data Quality: A Case Study from Japan. *Int. J. Cartogr.* **2019**, *5*, 214–224. [CrossRef]
38. Zhang, G.; Zhu, A.X. The Representativeness and Spatial Bias of Volunteered Geographic Information: A Review. *Ann. GIS* **2018**, *24*, 151–162. [CrossRef]
39. Hossain, M.D.; Chen, D. Segmentation for Object-Based Image Analysis (OBIA): A review of algorithms and challenges from remote sensing perspective. *ISPRS J. Photogramm. Remote Sens.* **2019**, *150*, 115–134. [CrossRef]
40. Ruff, L.; Görnitz, N.; Deecke, L.; Siddiqui, S.A.; Vandermeulen, R.A.; Binder, A.; Müller, E.; Kloft, M. Deep One-Class Classification. In Proceedings of the International Conference on Machine Learning, Stockholm, Sweden, 10–15 July 2018.